

# In-Place Rotation for Enhancing Snake-like Robot Mobility

Alexander H. Chang<sup>1</sup> and Patricio A. Vela<sup>1</sup>

**Abstract**—Gaits engineered for snake-like robots to rotate in-place instrumentally fill a gap in the set of locomotive gaits that have traditionally prioritized translation. This paper designs a Turn-in-Place gait and demonstrates the ability of a shape-centric modeling framework to capture the gait’s locomotive properties. Shape modeling for turning involves a time-varying continuous body curve described by a standing wave. Presumed viscous robot-ground frictional interactions lead to body dynamics conditioned on the time-varying shape model. The dynamic equations describing the Turn-in-Place gait are validated by an articulated snake-like robot using a physics-based simulator and a physical robot. The results affirm the shape-centric modeling framework’s capacity to model a variety of snake-like robot gaits with fundamentally different body-ground contact patterns. As an applied demonstration, example locomotion scenarios partner the shape-centric Turn-in-Place gait with a Rectilinear gait for maneuvering through constrained environments based on a multi-modal locomotive planning strategy. Unified shape-centric modeling facilitates trajectory planning and tracking for a snake-like robot to successfully negotiate non-trivial obstacle configurations.

## I. INTRODUCTION

Gait-based snake-like robot locomotion over flat ground has primarily focused on a handful of motion primitives: lateral undulation, sidewinding and rectilinear forms of motion. These gaits exhibit predominantly-translational movement. In application, they are used by snake-like robots to achieve large translational displacements (many body lengths) to reach prescribed goal positions. Steering during locomotion involves modulating gait parameters to induce steering effects [1]–[5]. For lateral undulation and rectilinear gaits, steering relies on joint offsets. For conical sidewinding, the cone half-angle mediates the turning rate. The steering parameters govern the robot’s body shape during locomotion and are subject to saturation limits. Beyond the limits, the prescribed body shape is not realizable, either due to actuator constraints or due to self-collision. Consequently, the curved trajectories resulting from these gaits are similarly subject to a saturating turning rate. There is a limit to how tightly the robot may turn under translation-dominant gaits.

Locomotive models for translational gaits have been derived as either dynamic or kinematic motion models. Derivations of lateral undulation and rectilinear models are specialized to the particular gait of interest and to the underlying snake-like robot design [6]–[8]. Follow-on trajectory control strategies are tied to the particular gait’s motion model, possibly with provable tracking guarantees [6]. Conical forms of sidewinding have been studied under the presumption

of ideally-static rolling body-ground contact. A kinematic analysis results in a closed-form motion model, parametrized with respect to the gait’s input shape parameters [9]. A re-parametrization allows this gait to be re-framed as a simple differential-drive vehicle, for which traditional path tracking approaches may then be applied [4]. Alternatively, a shape-centric modeling framework has been presented, whereby shape kinematics and locomotive dynamics of various bio-inspired gaits for snake-like robots are described through a unified modeling approach [5], [10]. Reduced-order motion models, that capture the time-averaged kinematic behavior of each gait, can be empirically-derived from the full system dynamics. Reduction of complex dynamics associated with snake-like robotic gaits, to simplified motion models, facilitates locomotive planning and control [5], [11]. This model reduction approach realizes the framework proposed in [12]. An attractive property of the shape-centric modeling framework is its ability describe a variety of gaits and to produce uniformly structured motion models for each. Planning and control strategies viable for one gait apply to other gaits modeled using this approach. This generalization is meaningful for snake-like robots, and potentially other bio-inspired robots; organisms that serve as bio-inspirational focus frequently exhibit several modes of locomotion to accommodate varying environmental situations [13], [14].

More recently, gaits for elongated-body, limbless robots have been designed that ‘rotate-in-place’. While no known snake species exhibit gaits that accomplish this motion profile, biological inspiration has been found in nematode worms, a different elongated-body and limbless organism [15]. A turn-in-place gait variant, designated ‘frequency turning’, has been discovered through an empirical search through the robot shape space [3], [16]. The net change in orientation achieved over a single cycle of these gaits is large, while net translation remains relatively small. Interestingly, the nematode worm-inspired Omega Turn relies solely on planar shape changes, with no vertical lift, to accomplish rotation; the latter frequency turning gait instead accomplishes this through strategic body-ground contact planning. Motion models for these gaits are grounded in the articulated platforms on which they are applied and involve elements of empirical sampling for different locomotion environments.

The unique motion profile characterizing turn-in-place gaits fills an important gap in the space of locomotive behaviors available to snake-like robots. Adding a turn-in-place gait to their toolbox realizes the ability to mimic differential-drive wheeled robots. As a consequence, planning and tracking control approaches frequently used on wheeled robots become more comprehensively applicable to snake-like robots. These wheeled platforms can steer while com-

1: The authors are with the School of Electrical and Computer Engineering, Georgia Institute of Technology, Atlanta, GA, USA. Email: alexander.h.chang@gatech.edu, pvela@ece.gatech.edu

This work was supported by NSF grant #1562911.

manding non-zero linear velocities, and can arbitrarily re-orient in-place at (near) zero linear velocity. In a similar manner, multi-modal switching between turn-in-place and translationally-focused gaits permit snake-like robots to traverse paths that neither gait alone may achieve. This greatly broadens set of nageable locomotion scenarios for snake-like robots, as candidate trajectory solutions are no longer constrained by turning rate limits.

**Contribution.** We design a Turn-in-Place gait for snake-like robots with standing wave shape kinematics. A shape-centric modeling framework [5] conditioned on the gait describes the robot’s locomotive dynamics. The gait is represented by a time-varying continuous body curve defined with respect to a static average body reference curve and rigid body frame. Planar group dynamics are derived for this continuous-body gait after introducing a strategically-engineered body-ground contact pattern and using a viscous friction model. The equations of motion are validated in a physics-based simulator (Gazebo) and on a physical snake-like robot. The validation highlights the shape-centric modeling framework’s capacity to describe a variety of snake-like robot gaits in a unified manner. The uniformly-structured gait models that result are useful in locomotion planning and control. Integrated use of the Turn-in-Place gait with a pre-existing Rectilinear gait leads to a multi-gait trajectory synthesis and tracking strategy. A snake-like robot can then traverse obstacle-strewn scenarios requiring tight turns by exploiting each gait’s affordances.

## II. TURN-IN-PLACE GAIT KINEMATICS

Recognizing the need for locomotion that goes beyond primarily translational movement for snake-like robots has led to the design of gaits with large angular and small translational displacements, i.e., turning in-place. Such gaits complement the gaits traditionally used for snake-like robot locomotion that achieve large translational displacements to follow reference paths and reach goal positions many body lengths distant. Two examples being the Omega Turn as engineered from biologically-inspired observations of worms [15], and ‘frequency turning’ as discovered through a parameter sweep of a parametrized gait [17]. Gait shapes associated with both are formulated as traveling waves and vary in their use of vertical lift to manage body-ground contact. Here, we design a Turn-in-Place gait from basic physical principles. A standing wave gait shape is coupled with a coordinated body-ground contact profile to generate periodic stepping motion, whereby each step rotates the snake in-place. Modeling of the gait dynamics employs a shape-centric modeling framework [5] to confirm Turn-in-Place movement.

The full 3-D gait shape is represented by a continuous-body curve,  $q(s, t; \bar{A})$ , defined relative to a reference body curve,  $\bar{q}(s; \bar{A})$ , and rigidly attached body frame. Analysis of the gait’s locomotive properties focuses on the gait shape projection of  $q(s, t; \bar{A})$  onto the plane of locomotion. This projected shape is denoted by  $r(s, t; \bar{A})$ . The component of  $q(s, t; \bar{A})$  describing vertical lifting of the body from the ground will be described by a body-ground contact profile, defined along  $r(s, t)$ . Under this model, design of the Turn-in-Place gait kinematics reduces to engineering a time-cyclical

body shape,  $r(s, t)$ , and a coordinated body-ground contact profile  $\mathcal{S}_{\text{cont}}(t)$ .

### A. Gait Shape

The Turn-in-Place gait shape description in the locomotion modeling plane,  $r(s, t; \bar{A})$ , is a sinusoidal standing wave; see Figure 1. Its planar shape is defined with respect to the reference body curve’s projection onto the locomotion plane,  $\bar{r}(s, t)$ . For this gait,  $\bar{r}(s, t)$  is a straight line parametrized with respect to arc length,  $s$ . The body frame  $g \in SE(2)$  is rigidly attached to the reference body at the center of the reference body where  $s = 0$ . The length of the reference body is  $L$  such that  $s \in [-\frac{L}{2}, \frac{L}{2}]$ . The Turn-in-Place gait standing wave is

$$r(s, t; \bar{A}) = \left[ A(t) \sin \left( 2\pi \cdot \frac{s}{\lambda(t)} \right) \right] \quad (1)$$

where

$$A(t) = \bar{A} \sin(\pi f t) \quad (2)$$

for peak amplitude  $\bar{A}$ , frequency  $f$  and corresponding gait period  $T = \frac{1}{f}$ . The wavelength,  $\lambda(t)$ , is a function of  $A(t)$  and the total fixed curve length  $\bar{L}$  (i.e., robot body length). It is computed by the root-finding operation,  $\lambda(t) = \text{root}_{\gamma} (\text{ArcLen}(r(s, t; A(t), \gamma)) - \bar{L})$ . The gait is designed to be a single sinusoidal standing wave,  $L(t) = \lambda(t)$ , periodic in time.

The robot begins each gait cycle in a straight-body configuration, illustrated in Figure 1a, where  $r(s, t)$  is denoted by the union of purple and green curve segments. Over the course of a half gait period, the shape transitions to a sine wave comprising a single wavelength,  $\lambda$  (Fig. 1b). During the second half of the gait cycle, this shape transitions back to a straight-body configuration (Fig. 1c).

The rigid reference frame and the gait shape define a set of local frames  $g_{\text{shape}}(s, t) \in SE(2)$  residing along the body curve  $r(s, t)$  whose local  $x$ -axis is tangent to the body curve. The frame decomposes into a rotation,  $R(s, t) \in SO(2)$ , and a translation,  $r(s, t) \in E(2)$ , specified relative to the rigid body frame,  $g$ .

A vertical body curve component,  $h(s, t)$ , dictates which segments of the body are in ground contact and when. It is constructed such that the segments in ground contact follow a desired contact schedule  $\mathcal{S}_{\text{cont}}(t)$ , in (3), for this gait. The full 3-D gait shape is described as,  $q(s, t; \bar{A}) = r(s, t; \bar{A}) + h(s, t)$ .

### B. Robot-Environment Contact

Vertical shape deformations of the snake-robot lead to desired robot-ground interaction forces. Here, the time-periodic body-ground contact pattern is engineered to promote in-plane rotation through a stepping pattern coupled to asymmetrical contact velocities. In reference to Figure 1, body-ground contact segments are illustrated as purple curves (green means no contact). The set of points along the body with ground contact is represented by (3), where  $\ell_{\text{cont}}(t)$  denotes the cyclically-varying length of each contact segment. Both contact segments maintain a minimum length  $\bar{\ell}_{\text{cont}}$ , and are centered about two points along the body, at  $s = 0, \frac{L}{2}$ .

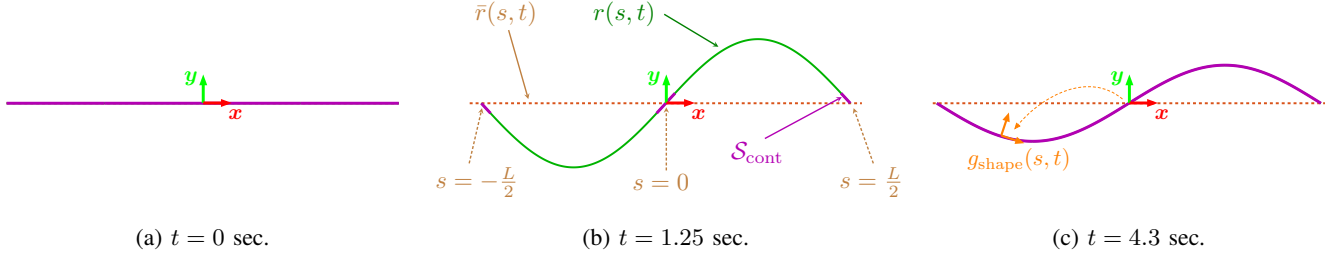


Fig. 1: Sequence of Turn-in-Place gait shapes and component curves, over the course of one gait cycle ( $T = 5$  sec.): reference body curve  $\bar{r}(s, t)$  (dashed brown); planar body curve  $r(s)$  (green+purple); body-ground contact segments  $\mathcal{S}_{\text{cont}}(t)$  (purple).

$$\mathcal{S}_{\text{cont}}(t) = \begin{cases} \{s \in [-\frac{\ell_{\text{cont}}}{2}, \frac{\ell_{\text{cont}}}{2}] \cup [\frac{L}{2} - \frac{\ell_{\text{cont}}}{2}, \frac{L}{2} + \frac{\ell_{\text{cont}}}{2}]\} & t \in [0, \frac{T}{2}) \\ \{s \in [-\frac{L}{2}, \frac{L}{2}]\} & t \in [\frac{T}{2}, T) \end{cases}, \text{ where } \ell_{\text{cont}}(t) = \max\left(\frac{L}{4}(1 + \cos(4\pi ft)), \bar{\ell}_{\text{cont}}\right) \quad (3)$$

A ground contact segment extending beyond the head of the body, at  $s = \frac{L}{2}$ , wraps-around to continue from the tail end, at  $s = -\frac{L}{2}$ .

Time-coordination between the gait shape  $r(s, t)$  in (1) and body-ground contact  $\mathcal{S}_{\text{cont}}(t)$  in (3) results in a robot motion pattern that appears like ‘rotational stepping’. The robot begins with a straight-body at the start of the gait. Over  $t \in [0, \frac{T}{2})$  it picks up interior segments of the body as  $r(s, t)$  evolves following a standing wave configuration with peak amplitude,  $\bar{A}$ . Over  $t \in [\frac{T}{2}, T)$  the entire body achieves ground contact as the gait shape recedes back to a straight-line configuration. This motion pattern produces a net change in orientation over a single gait cycle, with little translational displacement. We presume the Turn-in-Place gait evolves in a quasi-static manner; contact segments,  $\mathcal{S}_{\text{cont}}(t)$ , provide mechanical stability for the robot throughout the gait cycle.

### III. LOCOMOTIVE DYNAMICS

The shape-centric modeling approach for deriving the locomotive dynamics of prescribed gaits [5] applies to the Turn-in-Place gait. This section these dynamics to said gait.

The configuration space, for snake-like robots entails a a shape component,  $r \in M$ , and a group component,  $g \in SE(2)$ . The shape,  $r$ , is assumed to be fully controlled such that its dynamics are prescribed by  $u$ . Modeling emphasis is on the group dynamics of the robot, as influenced by its shape kinematics and external forces. Second-order dynamical equations that focus on the Lie group structure are

$$\begin{Bmatrix} \dot{r} \\ \dot{g} \\ \dot{p} \end{Bmatrix} = \begin{Bmatrix} u \\ g(\Omega^b - \mathcal{A}_{loc}(r, u)) \\ \text{ad}_{(\Omega^b - \mathcal{A}_{loc}(r, u))}^* p + \mathcal{F}^b(r, p, u) \end{Bmatrix}, \quad (4)$$

where  $u$  is the shape space control signal. The local principle connection  $\mathcal{A}_{loc}(r, u)$  splits the body velocity,  $\xi^b = g^{-1}\dot{g}$ , into horizontal and vertical components with  $\Omega^b$  denoting the vertical body velocity component and  $p = \mathbb{I}_{lock}(r)\Omega^b$  the vertical momentum. The horizontal body velocity  $\mathcal{A}_{loc}(r, u)$  describes free-space motion of the body due to shape kinematics. Vertical components are driven by external forcing. The net external wrench,  $\mathcal{F}^b$ , acts on the body frame and

models this external forcing. The dual adjoint operation captures Coriolis effects in the system.

Additional modeling elements must be computed to specialize the generalized dynamics to the Turn-in-Place gait. First, the locked inertia tensor associated with the gait is computed as,

$$\mathbb{I}_{lock}(r(s)) = \int_{-\frac{L}{2}}^{\frac{L}{2}} \begin{bmatrix} \mathbb{1} & \mathbb{J}(s) \\ -r^T(s)\mathbb{J} & r^T(s)r(s) \end{bmatrix} ds, \quad (5)$$

and describes the inertia associated with instantaneous gait shapes,  $r(s, t)$ . Another term denotes dynamic coupling between the robot shape and group components,

$$\mathbb{S}(r(s), \dot{r}(s)) = \int_{-\frac{L}{2}}^{\frac{L}{2}} \begin{bmatrix} R(s) \\ -r^T(s)\mathbb{J}R(s) \end{bmatrix} \dot{r}(s) ds \quad (6)$$

$R(s) \in SO(2)$  is the orientation of a local frame  $g_{\text{shape}}(s)$ , placed at  $r(s)$  with its  $x$ -axis tangent to the curve, and

$$\mathbb{J} = \begin{bmatrix} 0 & -1 \\ 1 & 0 \end{bmatrix}.$$

The local connection form  $-\mathcal{A}_{loc}(r(s), \dot{r}(s))$  is computed from these terms and describes free-space motion of the robot body frame due to internal shape changes,

$$\mathcal{A}_{loc}(r(s), \dot{r}(s)) = -(\mathbb{I}_{lock}(r(s)))^{-1} \mathbb{S}(r(s), \dot{r}(s)). \quad (7)$$

The total body velocity is,  $\xi^b = \Omega^b - \mathcal{A}_{loc}(r(s), \dot{r}(s))$ .

#### A. Body-Environment Forcing

We apply viscous friction to model robot-environment interactions. Coefficients  $\mu_b$ ,  $\mu_f$  and  $\mu_n$  denote resistance to posteriorly-, anteriorly- and laterally-directed motion of the body relative to the ground. At each point of body-ground contact,  $s$ , frictional forcing is computed in the local frame  $g_{\text{shape}}(s)$  located at  $r(s)$ :

$$f(s) = \begin{bmatrix} -(\mu_b H(-v_x(s)) + \mu_f H(v_x(s)))v_x(s) \\ -\mu_n v_y(s) \end{bmatrix}. \quad (8)$$

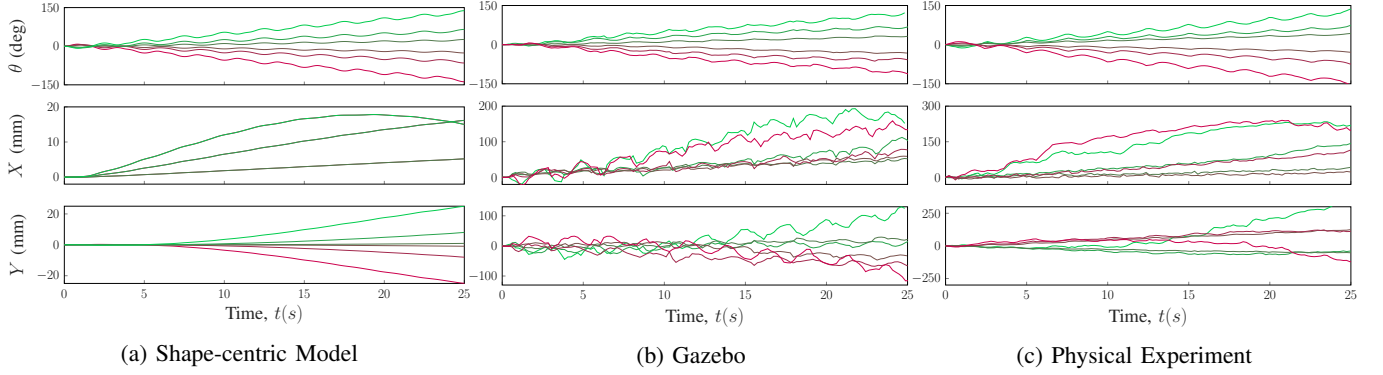


Fig. 2: Trajectories of the robot are tracked over a series of Turn-in-Place experiments, where the gait’s peak amplitude  $\bar{A}$  is varied from  $-120$  mm (red) to  $120$  mm (green). In each experiment, 10 gait cycles are run. A set of experiments is run in each of: **(a)** *shape-centric model* numerical integration, **(b)** *Gazebo simulation* and **(c)** *physical experiment*. In the latter two, the Turn-in-Place gait is implemented on a 12-link articulated snake-like robot.

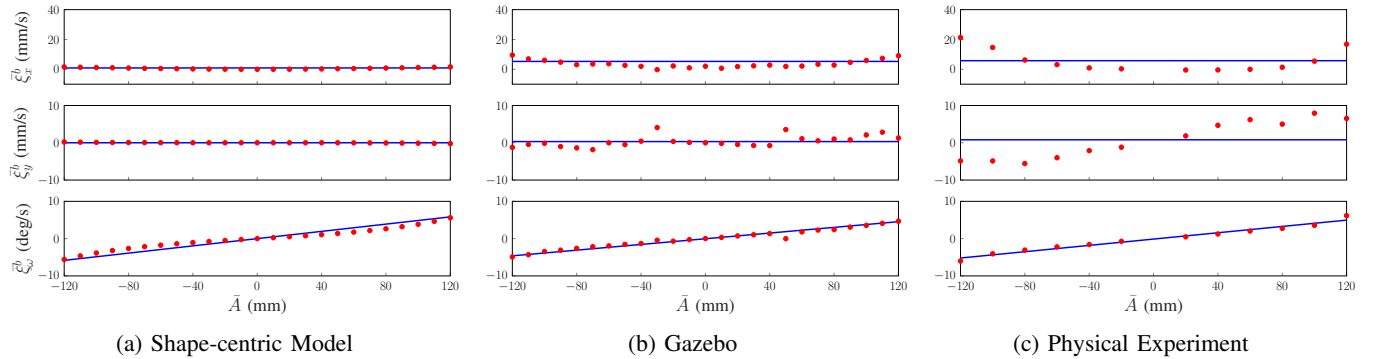


Fig. 3: Time-averaged, steady-behavior body velocities,  $\bar{\xi}^b$ , computed over 20 gait cycles of the Turn-in-Place gait, for a range of  $\bar{A}$ . This may alternatively be interpreted as a control-to-action map, denoted  $\Phi^{\text{TiP}}(\bar{A})$ . Red markers denote sampled values; blue plots represent linear fits. A set of experiments is run in each of: **(a)** *shape-centric model* numerical integration, **(b)** *Gazebo simulation* and **(c)** *physical experiment*. The latter two, entail a 12-link articulated snake-like robot.

$v(s) = [v_x(s) \ v_y(s)]^T$  describes velocity of the body at  $r(s)$  in the local frame  $g_{\text{shape}}(s)$ .  $H(\phi)$  denotes the Heaviside step function,

$$H(\phi) = \begin{cases} 0 & \phi \leq 0 \\ 1 & \phi > 0 \end{cases}. \quad (9)$$

Velocity at each point of body-ground contact,  $s \in \mathcal{S}_{\text{cont}}$ , expressed in the local frame at  $g_{\text{shape}}(s)$ , has contributions from body frame motion and the local shape derivative,

$$v(s) = \text{linear} \left( \text{Ad}_{g_{\text{shape}}(s)}^{-1} \xi^b \right) + R_{\text{shape}}^{-1}(s) \dot{r}(s). \quad (10)$$

Integration of external forcing acting along the body, after rigid translation to the body frame, produces the net wrench acting at the body frame,

$$\mathcal{F}^b = \int_{\mathcal{S}_{\text{cont}}} \left( \text{Ad}_{g_{\text{shape}}(s)}^{-1} \right)^T \cdot f(s) \, ds. \quad (11)$$

## B. Model Validation

The terms (5), (7) and (11) based on the Turn-in-Place gait shape equations (1) and (3), lead to a set of integro-differential equations for (4). We validate the equations using the Gazebo simulator and physical experiments, where the

Turn-in-Place gait is implemented on a 12-link articulated snake-like robot. Sweeping over a range of peak amplitude values,  $\bar{A}$ , and tracking the resulting body frame trajectories produces the plots in Figs. 2a, 2b, and 2c for the numerical integration of (4), Gazebo simulation, and robot implementation. Trajectories produced across the three experiment classes illustrate quantitatively consistent orientation trajectories and small net translation. Time-averaged body velocity measurements are plotted in Figure 3; angular velocity trends linearly and identically across the experiment classes.

Discrepancies occur in the translational outcomes of Figs. 2a-c (bottom 2 plots) and Figs. 3a-c (top 2 plots). Several circumstances lead to the differences. The articulated snake-like robot used in Gazebo simulation and physical experiment will have slightly different governing equations relative to the continuous body model employed in the shape-centric framework [5]. Additionally, the physical robot is designed to produce anisotropic friction between its body and ground [18], which results in the larger net translational displacements of Figs. 2c and 3c. Regardless, net translational displacement in all experiments remains small, less than half a body length over 10 gait cycles ( $\bar{L} = 800$  mm).

### C. Control-to-Action Behavior

At steady-behavior, the time-averaged body velocity of an undulatory gait is a useful characterization of its locomotive behavior. The time-averaged body velocity was measured for the Turn-in-Place gait in all 3 sets of experiments. After reaching a steady-state behavior, the three body velocity components were time-averaged over several gait cycles; see results depicted in Fig. 3. Time-averaged body velocities were measured (red markers) for a range of  $\bar{A}$  values, with the polynomial fit curve superimposed (blue).

The curve fit provides a closed-form, approximate representation of the time-averaged body velocity, as a function of  $\bar{A}$ . It defines a control-to-action map denoted as  $\Phi^{\text{TiP}}(\bar{A}) : \mathbb{R} \rightarrow \mathbb{R}^3$ . It maps the gait's input parameter,  $\bar{A}$ , to the resulting time-averaged body velocity twist  $\xi^b$ , and captures the gait's locomotive behavior as a kinematic motion model. This reduced motion model supports trajectory planning and tracking for snake-like robots (see §IV).

The Gazebo simulator regressed control-to-action map is

$$\Phi^{\text{TiP}}(\bar{A}) = \begin{bmatrix} 5.3 \text{ mm/s} \\ 0 \text{ mm/s} \\ -0.0382 \cdot \bar{A} + 0.0352 \text{ deg/s} \end{bmatrix}. \quad (12)$$

It entails a small positive forward bias, trivial lateral velocity, and linearly varying angular velocity (w.r.t.  $\bar{A}$ ). The range  $\bar{A} \in [-120, 120]$  mm reflects saturation limits based on the shapes achievable by the 12-link articulated snake-like robot.

### D. Shape-centric Modeling

The Turn-in-Place gait dynamics were derived using a shape-centric modeling approach [5]. The shape-centric modeling framework presents a unified approach to

- 1) define continuous-body shape kinematics, and
- 2) derive associated locomotive dynamics,

for gaits employed by limbless, elongated-body mobile robots. The modeling framework has been used to model a variety of gaits including a caterpillar-like rectilinear gait, lateral undulation, and sidewinding [5], [10]. Here, we demonstrate this modeling approach additionally describes the locomotive behavior of a very different gait: a turn-in-place motion primitive. Characterization of the gaits' steady-state locomotive behaviors leads to uniformly structured control-to-action maps. The reduced-order motion models simplify these gaits' dynamics to differential drive-like kinematic motion models useful for planning and control.

## IV. MULTI-GAIT TRAJECTORY PLANNING AND TRACKING

Multi-gait trajectory synthesis is accomplished using a three-pass approach to output a discrete-time reference trajectory with feed-forward controls. Each pass after the first incrementally refines the current trajectory. The final product is a controlled, switched-gait trajectory designed to move the robot from its starting pose to a prescribed goal position. Synthesis is specialized to the two gaits, Rectilinear and Turn-in-Place,  $\mathcal{MP} = \{\text{RL}, \text{TiP}\}$ . The Rectilinear gait employs a caterpillar-like, anteriorly-propagating body wave to produce

(predominantly) translational motion. Limited turning ability is accomplished by modulating the average (reference) body curvature  $\kappa$  [5]. Its control-to-action map in the Gazebo simulation environment is,

$$\Phi^{\text{RL}}(\kappa) = [36 \text{ mm/s}, 0 \text{ mm/s}, -1696.7 \cdot \kappa \text{ deg/s}]^T, \quad (13)$$

for  $\kappa \in [-1.5e-3, 1.5e-3] \text{ mm}^{-1}$ . Other gait parameters associated with the Rectilinear gait remain fixed: frequency ( $f^{\text{RL}} = -0.4 \text{ Hz}$ ), body wave amplitude ( $A^{\text{RL}} = 60 \text{ mm}$ ), wavelength ( $\lambda^{\text{RL}} = 390 \text{ mm}$ ). The Turn-in-Place control-to-action map is (12). The map captures locomotive behavior as a kinematic motion model, parametrized with respect to peak amplitude  $\bar{A}$ .

Trajectory synthesis starts with a collision-free input seed path  $\mathbf{G}^{\text{seed}}$  consisting of a sequence of coordinates connecting the robot's start pose and goal position, typically generated using one's traditional path planning approach [19] of choice. The path generated in this first pass is absent of any control or timing information and is not constrained by the robot's locomotive dynamics.

### A. Pass 2: Unicycle-based Trajectory Synthesis

Pass 2 parametrizes the path  $\mathbf{G}^{\text{seed}}$  with respect to time. Presuming a fixed arc length speed consistent with the Rectilinear gait, the path is re-sampled at a fixed number of Rectilinear gait periods,  $T^{\text{intvl}} = \bar{N}^{\text{RL}}/f^{\text{RL}}$ , where  $\bar{N}^{\text{RL}} = 2$ . This discrete-time path is the reference path for a model predictive control (MPC) output tracker based on a unicycle motion model whose inputs are linear and angular velocities,  $v^{\text{uni}}$  and  $\omega^{\text{uni}}$ . Additional constraints limit the unicycle model to motion that is collectively achievable by the gaits in  $\mathcal{MP}$ ,

$$v^{\text{uni}} \in [\Phi_x^{\text{RL}}(\kappa) - \epsilon, \Phi_x^{\text{RL}}(\kappa) + \epsilon] \wedge \omega^{\text{uni}} \in [\omega_{\min}^{\text{TiP}}, \omega_{\max}^{\text{TiP}}] \quad (14)$$

where

$$\omega_{\min}^{\text{TiP}} = \min_{\bar{A}} \Phi_{\omega}^{\text{TiP}}(\bar{A}) \text{ and } \omega_{\max}^{\text{TiP}} = \max_{\bar{A}} \Phi_{\omega}^{\text{TiP}}(\bar{A}). \quad (15)$$

The small constant  $\epsilon$  adds slack to assist with convergence to a solution. In summary, linear velocity is constrained to that achievable by the Rectilinear gait, while the Turn-in-Place gait defines allowable angular velocities.

The output is  $(\mathbf{G}^{\text{uni}}, \mathbf{t}^{\text{uni}}, \mathbf{U}^{\text{uni}})$ , a collection of sets each of which has cardinality  $N^{\text{uni}}$ .  $\mathbf{G}^{\text{uni}} = \{g_i^{\text{uni}} \in SE(2)\}_{i=1}^{N^{\text{uni}}}$  is a sequence of pose coordinates. A corresponding time schedule  $\mathbf{t}^{\text{uni}}$  consists of timestamps at intervals of  $T^{\text{intvl}}$  seconds. Lastly,  $\mathbf{U}^{\text{uni}} = \{(v_i^{\text{uni}}, w_i^{\text{uni}})\}_{i=1}^{N^{\text{uni}}}$  are the open-loop control inputs for achieving the pose sequence  $\mathbf{G}^{\text{uni}}$ .

### B. Pass 3: Multi-gait Refinement

Pass 3 further revises the sets based on which gaits in  $\mathcal{MP}$  will realize the desired displacements. Stepping through each trajectory point  $i = 1 \dots N^{\text{uni}}$ , the ability of the Rectilinear gait to apply the associated open-loop control is tested:

$$\text{isRLTraversable}(i) = (\omega_i^{\text{uni}} \leq 0.85 \cdot \omega_{\max}^{\text{RL}}) \quad (16)$$

for the maximum angular velocity of the Rectilinear gait,

$$\omega_{\max}^{\text{RL}} = \max_{\kappa} \Phi_{\omega}^{\text{RL}}(\kappa). \quad (17)$$

Trajectory points satisfying (16) entail feasible angular velocities  $\omega_i^{\text{uni}}$  for the Rectilinear gait using an average (reference) body curvature  $\kappa_i = (\Phi_\omega^{\text{RL}})^{-1}(\omega_i^{\text{uni}})$ .

Trajectory segments where (16) is false are presumed infeasible for the Rectilinear gait. The robot will employ a Turn-in-Place, Rectilinear, Turn-in-Place gait sequence to negotiate them. A trajectory segment *not* satisfying (16), beginning at point  $j$  and ending at point  $k > j$ , is circumvented by connecting a straight line between the two points; we denote this line's spatial orientation as  $\theta_{j \rightarrow k}$ . At point  $j$ , a series of 6 Turn-in-Place gait cycles (trajectory points) is inserted to close the error,  $\theta_{j \rightarrow k} - \theta_j^{\text{uni}}$ , with an angular velocity  $\omega^{\text{MG}} = \frac{(\theta_{j \rightarrow k} - \theta_j^{\text{uni}}) \cdot f^{\text{TiP}}}{6}$ . Following this, we insert a series of Rectilinear gait cycles to traverse the distance from  $g_j^{\text{uni}}$  to  $g_k^{\text{uni}}$ , with the Rectilinear turning parameter fixed to  $\kappa = 0$ ; the number of Rectilinear gait cycles inserted is dictated by the fixed speed at which the gait travels,  $\Phi_x^{\text{RL}}(\kappa)$ . At  $g_k^{\text{uni}}$ , a final sequence of 6 Turn-in-Place gait cycles is inserted to close the remaining orientation error,  $\theta_k^{\text{uni}} - \theta_{j \rightarrow k}$ , with angular velocity  $\omega^{\text{MG}} = \frac{(\theta_k^{\text{uni}} - \theta_{j \rightarrow k}) \cdot f^{\text{TiP}}}{6}$ . Turn-in-Place input parameters needed to achieve a desired angular velocity are  $\bar{A} = (\Phi_\omega^{\text{TiP}})^{-1}(\omega)$ .

The refined multi-gait trajectory is described by the collection,  $(\mathbf{G}^{\text{MG}}, \mathbf{t}^{\text{MG}}, \mathbf{MP}^{\text{MG}}, \mathbf{U}^{\text{MG}})$ . Each set in the collection is of cardinality  $N^{\text{MG}}$ , the total number of points in the refined multi-gait trajectory.  $\mathbf{G}^{\text{MG}}$  and  $\mathbf{t}^{\text{MG}}$  denote planned pose coordinates and time, respectively.  $\mathbf{MP}^{\text{MG}} = \{mp_i^{\text{MG}} \in \mathcal{MP}\}_{i=1}^{N^{\text{MG}}}$  expresses the gait sequence designed to traverse  $\mathbf{G}^{\text{MG}}$ , while  $\mathbf{U}^{\text{MG}} = \{\beta_i^{\text{MG}} \in \mathbb{R}\}_{i=1}^{N^{\text{MG}}}$  contains the gait-specific input parameter to be commanded at each trajectory point.  $\beta_i^{\text{MG}}$  describes either Rectilinear curvature  $\kappa_i^{\text{MG}}$  or Turn-in-Place peak amplitude  $\bar{A}_i^{\text{MG}}$ , when  $mp_i^{\text{MG}} = \text{RL}$  or  $\text{TiP}$ , respectively.

### C. Trajectory Tracking

Tracking of the multi-gait trajectory is accomplished using simple proportional feedback control. Feedback control is computed at scheduled time intervals, specified in  $\mathbf{t}^{\text{MG}}$ . We denote the waypoint being tracked by its index  $i = 1 \dots N^{\text{MG}}$ . The pose error associated with any waypoint  $g_i^{\text{MG}} \in \mathbf{G}^{\text{MG}}$  and robot pose  $g$  is  $g_{\text{err}} = g^{-1} \cdot g_i^{\text{MG}}$ . It is the the waypoint frame  $g_i^{\text{MG}}$  relative to the actual robot frame. Individual translational and rotational errors,  $(x_{\text{err}}, y_{\text{err}}, \theta_{\text{err}})$ , are extracted.

Feedback-correction is dependent upon the planned gait  $mp_i$ , at a each waypoint  $i$ ,

$$\omega_{\text{fb}} = \begin{cases} k_\theta^{\text{RL}} \cdot \theta_{\text{err}} + k_y^{\text{RL}} \cdot y_{\text{err}}, & mp_i = \text{RL} \\ k_\theta^{\text{TiP}} \cdot \theta_{\text{err}}, & mp_i = \text{TiP} \end{cases}. \quad (18)$$

The open-loop gait parameter,  $\kappa_i^{\text{MG}}$  or  $\bar{A}_i^{\text{MG}}$ , is incorporated as a feed-forward value in the applied control,

$$\kappa_{\text{fb}} = (\Phi_\omega^{\text{RL}})^{-1}(\Phi_\omega^{\text{RL}}(\kappa_i^{\text{MG}}) + \omega_{\text{fb}}), \quad mp_i = \text{RL} \quad (19)$$

$$\bar{A}_{\text{fb}} = (\Phi_\omega^{\text{TiP}})^{-1}(\Phi_\omega^{\text{TiP}}(\bar{A}_i^{\text{MG}}) + \omega_{\text{fb}}), \quad mp_i = \text{TiP} \quad (20)$$

As the robot proceeds sequentially through the planned waypoints, in  $\mathbf{G}^{\text{MG}}$ , the forward error is assessed. If it

exceeds a threshold,  $x_{\text{err}} > \bar{d}_{\text{err}}$ , the relevant target waypoint  $i$  is *not* incremented; the robot continues tracking the same waypoint until forward error falls below  $\bar{d}_{\text{err}}$ .

## V. LOCOMOTION SCENARIOS

This section pairs the Turn-in-Place gait with a translation-dominant Rectilinear gait and show that a 12-link snake-like robot can plan and track trajectories that neither gait alone is capable of following. Three locomotion scenarios, depicted in Fig. 4, are successfully completed using these two gaits within the multi-gait trajectory planning and tracking approach presented in §IV. Rectilinear motion is used for path segments that require little steering. The multi-gait planner switches to Turn-in-Place motion at “sharp” corners and is used at the start of each trajectory to align the robot body frame with the direction of travel.

Taken together the scenarios require sufficiently diverse motion profiles that they can be deemed reflective of most navigation scenarios with comparable free space vs collision space characteristics. The narrowest passageways have widths equivalent to the robot body length ( $\bar{L} = 800$  mm). Tracking errors arise due to initial transients when momentum accumulates, transitions when gait parameter values change, and gait switching. These effects are un-modeled and are not considered as part of the multi-gait trajectory synthesis process. Discrete-time, trajectory tracking control corrects for these errors.

The control and orientation signals are plotted in Figure 5. Their piecewise nature is a function of the active gait changing as a function of time, and therefore the applied control for the gait. Whereas Figure 4 confirms trajectory tracking, Figure 5 confirmed orientation tracking (top left graph for each scenario). Closed-loop discrete control under the empirically regressed models successfully tracks the synthesized trajectories to arrive at the goal point.

## VI. CONCLUSION

The paper described Turn-in-Place gait for snake-like robots, whose standing wave and body-contact properties were engineered to primarily produce net rotational motion. The rigid dynamics of the body frame were derived using a shape-centric modeling framework [5] with viscous body-ground friction. Validation of the resulting integro-differential dynamical equations employed the Gazebo simulator and physical experiments for a 12-link articulated robot.

The Turn-in-Place gait is the fourth motion primitive whose evolution the shape-centric modeling approach is capable of describing. It is further evidence that the framework constitutes a unified modeling approach for describing the locomotive behavior of a variety of gaits for snake-like robots. In characterizing each gait's time-averaged movement, we obtain a reduced-order control-to-action map describing each gait's steady-state locomotive behavior as a function of its input shape parameters. The maps resemble unicycle-like motion profiles such that planning and control frameworks commonly used for differential-drive vehicles apply to the snake-like robot. Pairing the Turn-in-Place gait with a previously modeled Rectilinear gait in a multi-gait planning

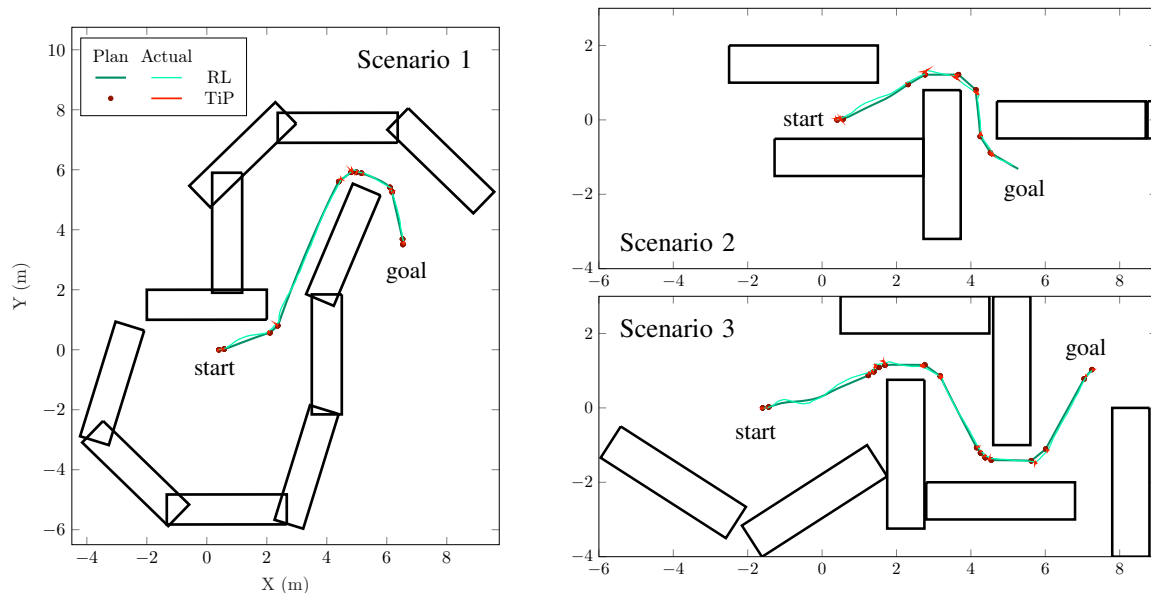


Fig. 4: Depiction of environments for the three locomotion scenarios, with parametric plots of the multi-gait planned and achieved (based on tracking) trajectories. The snake-like robot successfully maneuvers to the goal in all cases.

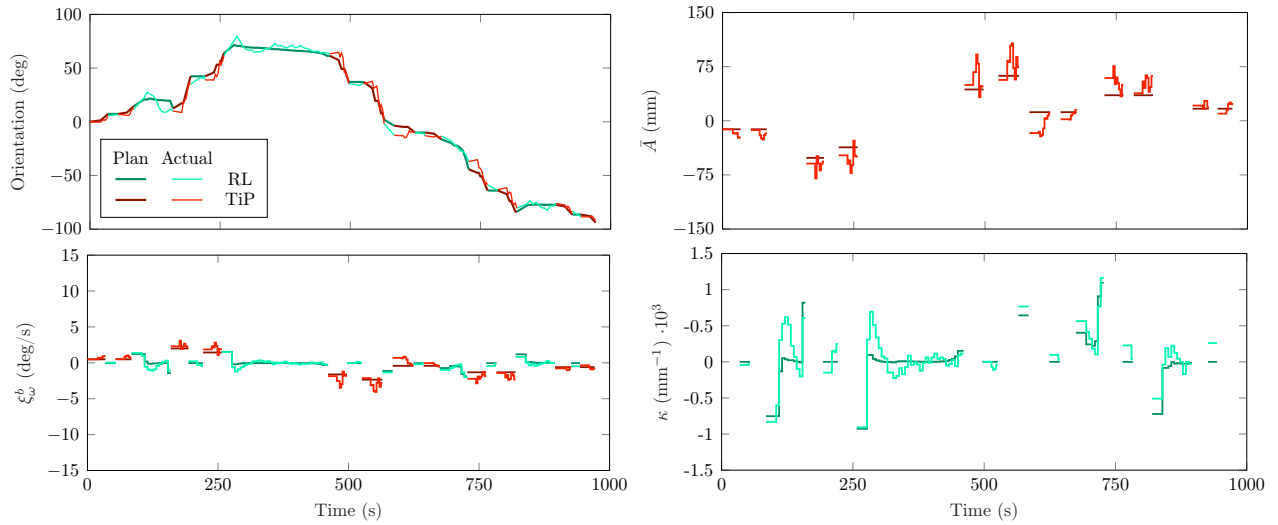
and tracking strategy permits traversal through environments requiring high angular displacements. The snake-like robot successfully tracks multi-gait trajectory plans, in Gazebo simulation, to complete several navigation scenerios.

The Turn-in-Place gait fills a critical gap in the space of motion profiles achievable by snake-like robots. The utility of rotating in-place is evident in the locomotion scenarios demonstrated here. By filling this mobility gap, a greater breadth of planning and tracking control approaches, commonly used for differential-drive vehicles, become applicable for snake-like robot locomotion. Future work aims to replicate the simulations on the physical robot, once a means to track its pose over long distances has been established.

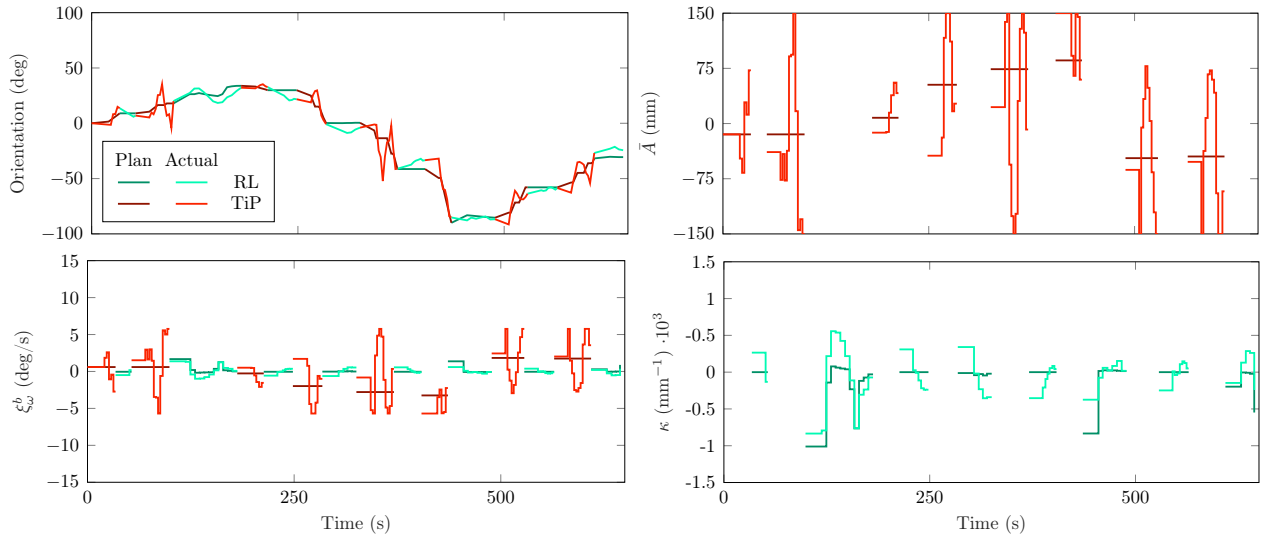
#### REFERENCES

- [1] A. M. Kohl, E. Kelasidi, A. Mohammadi, M. Maggiore, and K. Y. Pettersen, "Planar maneuvering control of underwater snake robots using virtual holonomic constraints," *Bioinspiration and Biomimetics*, vol. 11, 2016.
- [2] W. Yang, G. Wang, and Y. Shen, "Efficient and smooth enhanced curve path following of underactuated snake robots," in *AIM*, 2019, pp. 175–180.
- [3] H. Astley, C. Gong, M. Travers, M. Serrano, P. Vela, J. M. III, H. Choset, D. Hu, and D. Goldman, "Modulation of orthogonal body waves enables high maneuverability in sidewinding locomotion," *Proceedings of the National Academy of Sciences*, vol. 112, no. 19, pp. 6200–5, 2015.
- [4] X. Xiao, E. Cappel, W. Zhen, J. Dai, K. Sun, C. Gong, M. Travers, and H. Choset, "Locomotive reduction for snake robots," in *ICRA*, 2015, pp. 3735–3740.
- [5] A. Chang and P. Vela, "Shape-centric modeling for control of traveling wave rectilinear locomotion on snake-like robots," *Robotics and Autonomous Systems*, vol. 124, p. 103406, 2020.
- [6] P. Liljebäck, K. Pettersen, Ø. Stavdahl, and J. Gravdahl, *Snake Robots: Modelling, Mechatronics, and Control*. Springer, 2013.
- [7] W. Tang, F. Reyes, and S. Ma, "Study on rectilinear locomotion based on a snake robot with passive anchor," in *IROS*, 2015, pp. 950 – 955.
- [8] W. Tang and S. Ma, "Analysis of rectilinear motion of a three-segment snake robot under action of dry friction," in *ICRA*, 2015, pp. 3723–3728.
- [9] C. Gong, R. L. Hatton, and H. Choset, "Conical sidewinding," in *ICRA*, 2012, pp. 4222–4227.
- [10] A. Chang, M. Serrano, and P. Vela, "Shape-centric modeling of lateral undulation and sidewinding gaits for snake robots," in *CDC*, 2016, pp. 6676 – 6682.
- [11] A. H. Chang, N. P. Hyun, E. I. Verriest, and P. A. Vela, "Optimal trajectory planning and feedback control of lateral undulation in snake-like robots," in *ACC*, 2018, pp. 2114–2120.
- [12] K. A. McIsaac and J. P. Ostrowski, "A framework for steering dynamic robotic locomotion systems," *International Journal of Robotics Research*, vol. 22, no. 2, pp. 83–97, 2003.
- [13] R. J. Lock, R. Vaidyanathan, S. C. Burgess, and J. Loveless, "Development of a biologically inspired multi-modal wing model for aerial-aquatic robotic vehicles through empirical and numerical modelling of the common guillemot, uria aalge," vol. 5, no. 4, p. 046001, Nov 2010.
- [14] K. H. Low, T. Hu, S. Mohammed, J. Tangorra, and M. Kovac, "Perspectives on biologically inspired hybrid and multi-modal locomotion," vol. 10, no. 2, p. 020301, Mar 2015.
- [15] T. Wang, B. Chong, K. Diaz, J. Whitman, H. Lu, M. Travers, D. I. Goldman, and H. Choset, "The omega turn: A biologically-inspired turning strategy for elongated limbless robots," in *IROS*, 2020, pp. 7766–7771.
- [16] C. Gong, M. Travers, H. Astley, D. Goldman, and H. Choset, "Limbless locomotors that turn in place," in *ICRA*, 2015, pp. 3747–3754.
- [17] J. Dai, M. Travers, T. Dear, C. Gong, H. C. Astley, D. I. Goldman, and H. Choset, "Robot-Inspired Biology: The Compound-Wave Control Template," in *ICRA*, 2015, pp. 5879–5884.
- [18] A. Chang and P. Vela, "Evaluation of bio-inspired scales on locomotion performance of snake-like robots," *Robotica*, vol. 37, no. 8, 2019.
- [19] J.-C. Latombe, *Robot Motion Planning*. USA: Kluwer Academic Publishers, 1991.

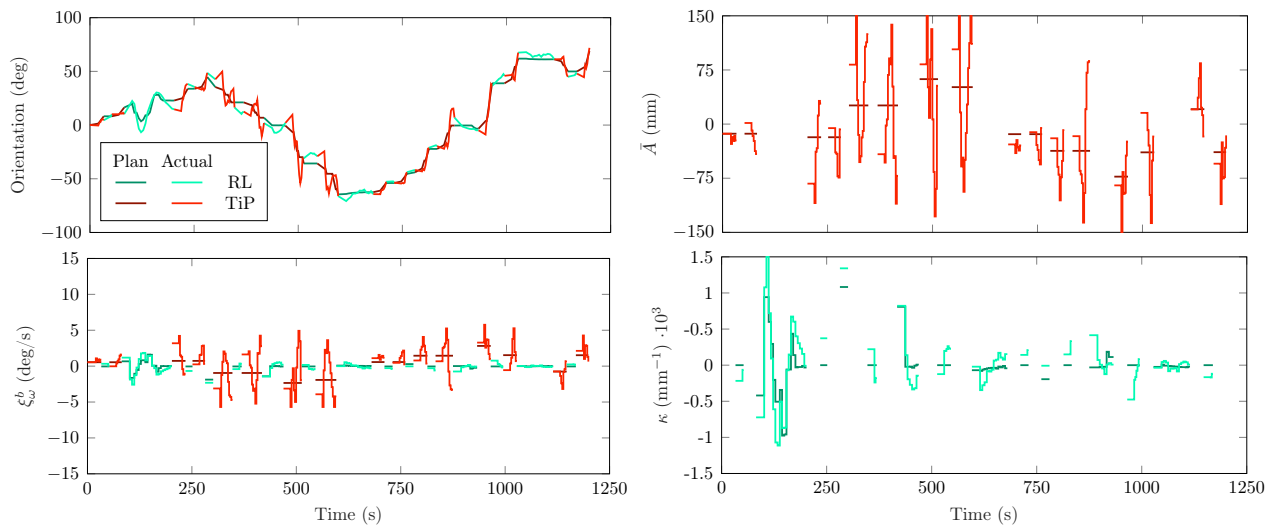




(a) Scenario 1 signals



(b) Scenario 2 signals



(c) Scenario 3 signals.

Fig. 5: Time-varying signals describing Scenarios 1-3 in Figure 4: **(top-left)** orientation,  $\theta(t)$  **(bottom-left)** angular velocity,  $\xi_{\omega}^b(t)$  **(top-right)** Rectilinear curvature,  $\kappa(t)$  **(bottom-right)** Turn-in-Place peak amplitude,  $\bar{A}(t)$ .